CASE STUDY OF NEARSHORE CURRENTS HAZARD ANALYSIS FOR RECREATIONAL BEACH DEVELOPMENT

Clint Chester M. Reyes[1], Eric C. Cruz[2], and Jose Carlo Eric L. Santos[3]

Nearshore current generation at two coastlines contemplated for beach resort development is studied with the use of a numerical model for coexisting waves and currents. A nested-mesh technique was applied to consolidate the 2 domains of coarse and fine bathymetric data and to translate deep water wave conditions at the nearshore mesh boundary. The hydrodynamic model is validated using tide data at the nearest tide stations, while offshore wave conditions, determined from a wave hindcasting method, are inputted as quasi-stationary forcing. Simulations results of wave-current co-existing fields indicate local areas of rip currents within the project coastlines. In order to evaluate the safe swimming zones, an analysis of threshold currents under idealized conditions of human characteristics was carried out, that indicated a threshold of 0.16 mps for pure currents. With a safety margin to account for co-existing waves, rip current zones not exceeding 0.1 mps are considered safe and are used to designate the safe swimming areas for the 2 locations.

Keywords: nearshore currents, rip currents, Palawan, Philippines, threshold current, waves

INTRODUCTION

In conjunction with a coastal resort and beach development project along the elongated island of Palawan, two beach coasts facing the West Philippine Sea are exposed to varying swells and wind waves throughout the entire year. The project areas are considered based on their observed suitability for recreational beach activities. In order to quantify and further assess the possible hazards and risk, several analyses are necessary, including nearshore currents, prevailing waves, and the extent and effect of storm surges within and at the local vicinities of the study areas.

The project areas are situated along the central western coastline of Palawan Island, Philippines. Interestingly, these two locations are located on the same side of Palawan and are situated relatively near each other but are subject to different wave and tidal forcing. Figure 1 shows these two locations as described. Location 1 is a 3.2-km-long coastline that is surrounded by islands and the adjacent coasts, while Location 2 is a 1.2-km-long coastline, which is part of a long and straight wave-exposed beach, around 8 km North of Location 1.

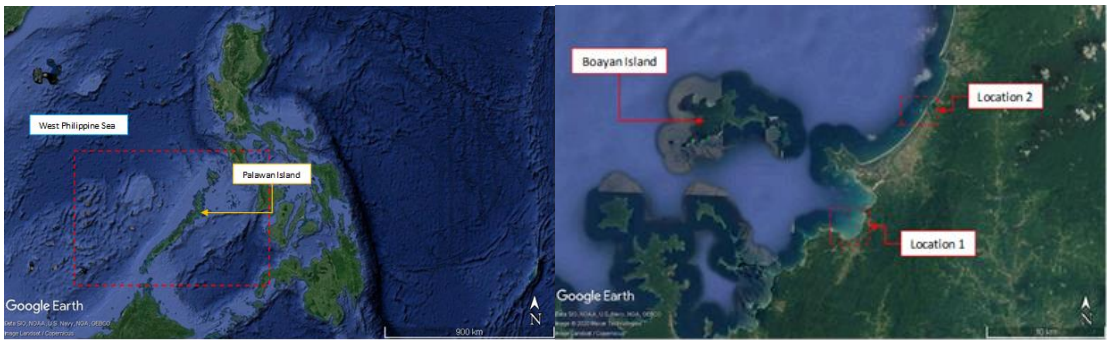

Figure 1. Philippines and Palawan Island, and focused image of Locations 1 and 2

AREA AND SITE BATHYMETRY

Nautical charts near the project area were gathered and consolidated to form a regional bathymetric model which extends out to the West Philippine Sea. In addition to this, a local higher resolution bathymetric survey at the project foreshore was also conducted to resolve necessary features that may

[1] Design Engineer, AMH Philippines Inc., Rm 205 Ang Bahay ng Alumni, Magsaysay Ave., Diliman, Quezon City, NCR, 1101, Philippines
[2] Ph D., Coastal Engineering Laboratory, University of the Philippines, Diliman, Quezon City, NCR, 1101, Philippines
[3] Principal Engineer, AMH Philippines Inc., Rm 205 Ang Bahay ng Alumni, Magsaysay Ave., Diliman, Quezon City, NCR, 1101, Philippines

affect nearshore wave transformation and wave-current interaction. The consolidated nearshore bathymetry of Locations 1 and 2 is shown below Figure 2).

Prevalent features of Location 1 include curvature of the coastline and a natural groin at the middle of the property composed of coralline and sandy material, which fully emerges during low tide and is submerged during high tide. Also, this area is heavily sheltered by islands, protecting the coast from waves coming from the West to the NW directions. Location 2 on the other hand, is composed of a straight coastline facing the NW, with large basaltic natural rock formations along the coast, including a rocky islet which forms a tombolo of sand at the rear. The coastline of Location 2 is located at the center of a longer coastline between 2 headlands separated by about 11 km.

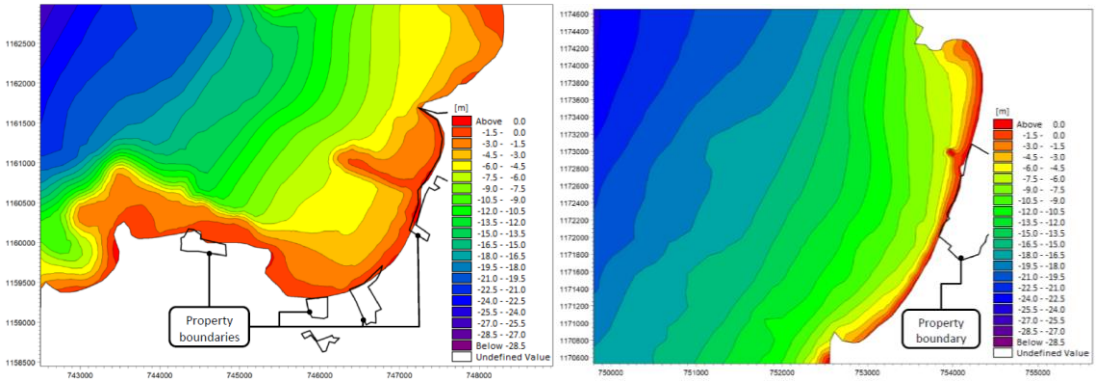

Figure 2. Bathymetric model nearshore of Location 1 and Location 2

NEARBY TIDE AND WIND STATIONS

Prior to conducting detailed analysis, preliminary data on water levels are necessary for model calibration. In addition, tidal statistics were also obtained for the simplification of tidal extremes in numerical analysis. Historical wind rose data at the offshore boundary is also necessary, which is used to hindcast wave data to serve as boundary conditions for the wave model in the absence of actual wave data.

The project area is closest to two local tide stations, namely, El Nido and Penascosa (Figure 5). These two tide stations provided the data for model calibration of the hydrodynamic model to be used. El Nido tide station is determined to be closer to the project area, although this tide station is sheltered by other islands. Hence, the Peñascosa station, which is more exposed to the West Philippine Sea, better represents the tidal fluctuations at the project area. The mean tidal range at this station is 1.08 m. Annual wind data was obtained from Pagasa Island located in the West Philippine Sea (Figure 6), approximately 500 km west of the project area. As seen in the annual wind rose diagram, strong winds up to 16 mps are observed from prevailing wind directions of northeast and southwest which occur during the Amihan and Habagat seasons, respectively.

Table 1. Tide statistics of the nearest tide stations

Station	Tide elevation (m)				
	MHHW	MHW	MTL	MLW	MLLW
Penascosa	0.56	0.41	0	-0.40	-0.52
El Nido	0.54	0.45	0	-0.45	-0.54

METHODOLOGY

NUMERICAL MODEL

The model domain is interpolated based on the consolidated coarse to fine bathymetric data, into an unstructured mesh for numerical simulations, which extend past the Spratly archipelago where secondary wind data is obtained (Figure 8). The hydrodynamic model is based on the nonlinear shallow

water equations (1,2) coupled with a spectral wave model derived from the wave action conservation equations (3,4). Considerations on wind friction, viscous effects, Coriolis forcing, bottom friction and depth-induced breaking are included in the coupled numerical model. Coupling of a hydrodynamic model with a wave model was deemed necessary in order to observe current-wave interaction at the project nearshore, which is highly varying given the changing waves and winds in both short-term and long-term seasonality. A similar approach was used by Bruneau et al. (2011) who modeled nearshore currents using a finite structured grid.

Figure 3. Nearby tide stations (NAMRIA)

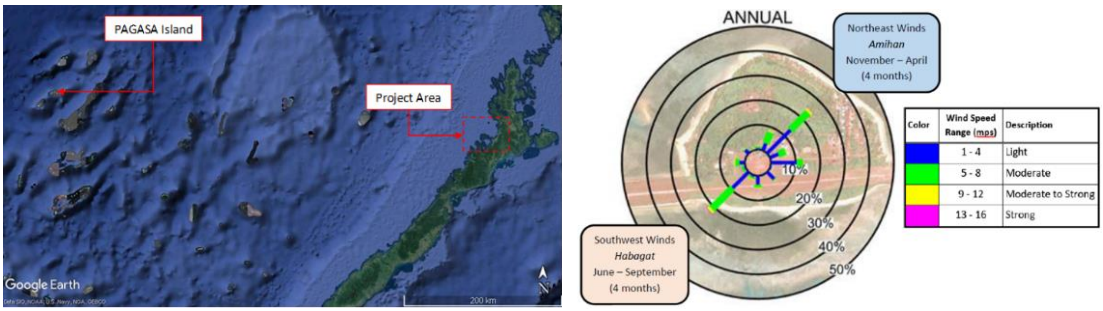

Figure 4. Location of Pagasa Island wind station relative to the project area

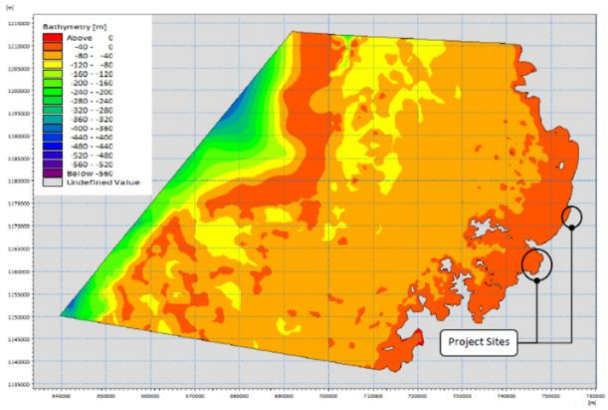

Figure 5. FEM depth-adaptive mesh for sea hydrodynamics computational domain

$$\frac{\partial \zeta}{\partial t} + \frac{\partial p}{\partial x} + \frac{\partial q}{\partial y} = \frac{\partial d}{\partial t} \tag{1}$$

$$\frac{\partial p}{\partial t} + \frac{\partial}{\partial x}\left(\frac{p^2}{h}\right) + \frac{\partial}{\partial y}\left(\frac{pq}{h}\right) + gh\frac{\partial \zeta}{\partial x} + \frac{gp\sqrt{p^2+q^2}}{C^2 h^2} - \frac{1}{\rho_w}\left[\frac{\partial}{\partial x}(h\tau_{xx}) + \frac{\partial y}{\partial x}(h\tau_{xy})\right] - \Omega q - fVV_x + \frac{h}{\rho_w}\frac{\partial}{\partial x}(p_a) = 0 \tag{2}$$

$$\frac{\partial N}{\partial t} + \nabla \cdot (\vec{v}\mathrm{N}) = \frac{S}{\sigma} \tag{3}$$

$$(c_x, c_y) = \frac{d\vec{x}}{dt} = \overrightarrow{c_g} + \vec{U} \tag{4}$$

$$c_\sigma = \frac{d\sigma}{dt} = \frac{\partial\sigma}{\partial d}\left[\frac{\partial d}{\partial t} + \vec{U}\cdot\nabla_{\vec{x}} d\right] - c_g\vec{k}\cdot\frac{\partial\vec{U}}{\partial s}$$

$$c_\sigma = \frac{d\sigma}{dt} = \frac{\partial\sigma}{\partial d}\left[\frac{\partial d}{\partial t} + \vec{U}\cdot\nabla_{\vec{x}} d\right] - c_g\vec{k}\cdot\frac{\partial\vec{U}}{\partial s}$$

$$c_\theta = \frac{d\theta}{dt} = -\frac{1}{k}\left[\frac{\partial\sigma}{\partial d}\frac{\partial d}{\partial m} + \vec{k}\cdot\frac{\partial\vec{U}}{\partial \mathrm{m}}\right]$$

where,
$h(x,y,t)$ water depth ($=\zeta - d$, m)
$d(x,y,t)$ time varying water depth (m)
$\zeta(x,y,t)$ surface elevation (m)
$p,q(x,y,t)$ flux densities ($m^3/s/m$)
u,v depth averaged (m/s)
$C(x,y)$ Chezy resistance ($m^{1/2}/s$)
$f(V)$ wind friction factor (-)
$V, Vx, Vy(x,y,t)$ wind speed (m/s)
$\Omega(x,y)$ Coriolis parameter (m^{-1})
$p_a(x,y,t)$ Atmospheric pressure (N/m^2)
ρ_w density of water (kg/m^3)
τ_{xx}, τ_{xy}, τ_{yy} effective shear stress (N/m^2)
$N(\vec{x},\sigma,\theta,t)$ action density (Ns/m)
t time (s)
$\vec{x}$ = (x, y) Cartesian coordinates (m)
$\vec{v}$ = $(c_x, c_y, c_\sigma, c_\theta)$ propagation velocity (m/s, rad/s)
S source term (N/m)
$c_x, c_y, c_\sigma, c_\theta$ characteristic propagation speeds (m/s)
s space coordinate (m)
θ wave direction (radian)
m coordinate perpendicular to s (m)

BOUNDARY CONDITIONS

In order to determine offshore wave conditions which, act at the model boundary, wind data from Pagasa Island was used to hindcast offshore waves. The methodology used is similar to the wave hindcasting done by Cruz et al (2018) which used annual wind rose data and determined the effective fetch from each cardinal direction following Saville (1954). This method uses a weighted sum of adjacent fetch lines at 6-degree intervals up to 45 degrees in both clockwise and counterclockwise directions.

$$F_{eff} = \frac{\sum F_i \cos^2\theta_i}{\sum \cos\theta_i} \tag{5}$$

where,
F_i fetch distance
θ_i angle from main wind direction

Generally, raw wind data obtained from wind stations are obtained at varying locations based on the elevation of the wind station. For this case study, windspeeds were transformed to a 10-m elevation as prescribed by the Coastal Engineering Manual (USACE, 2006), shown below.

$$U_{10} = U_z\left(\frac{10}{z}\right)^{1/7} \tag{6}$$

where,
z elevation of measurement
U_z wind velocity at elevation z

Boundary wave heights and periods were then hindcasted from the determined fetch and wind speeds and directions. This was performed using the hindcast equations proposed by Sverndrup et al (1947) and revised by Bretschneider (1951, 1958). This SMB method is recommended in coastal engineering manuals like the Philippines Ports Authority – Port Standards Manual (2005). The results obtained from these equations are summarized in Table 2. It is seen that the highest offshore waves reach up to 6.17 m with periods of 9.37 s coming from the WSW direction, while the most frequent waves are coming from the northeast, which is known to be the Amihan season generally occurring from the months of November to April, with height of up to 3.47 m and wave periods of 6.78 s. Other critical directions range from southwest to west, which is considered the second most frequent direction while also being one of the strongest.

$$\frac{gH_s}{U^2} = 0.30\left[1 - \frac{1}{\left\{1 + 0.004\left(\frac{gF_{eff}}{U^2}\right)^{\frac{1}{2}}\right\}^2}\right]$$
$$\frac{gT_s}{2\pi U} = 1.37\left[1 - \frac{1}{\left\{1 + 0.008\left(\frac{gF_{eff}}{U^2}\right)^{\frac{1}{3}}\right\}^5}\right] \quad (7)$$

where,
H_s significant wave height (m)
T_s significant wave period (s)
U wind velocity at 10 m above the sea surface (m/s)

Table 2. Offshore wave conditions

Direction	Velocity Range (m/s)	Annual Occurrence (%)	Feff (km)	Hso (m)	Tso (sec)	Hs rank
NE	1-4.0	24.7	89.94	0.39	2.67	5th highest wave
	5-8.0			1.41	4.65	
	8-12.0			2.74	6.14	
	12-16.0			3.47	6.78	
NNE	1-4.0	8.2	163.81	0.43	2.89	6th highest wave
	5-8.0			1.67	5.22	
	8-12.0			3.37	7.03	
N	1-4.0	1.4	212.75	0.44	2.98	4th highest wave
	5-8.0			1.79	5.47	
	8-12.0			3.67	7.44	
NNW	1-4.0	0.3	272.74	0.46	3.06	Non-critical
	5-8.0			1.89	5.71	
NW	1-4.0	2.2	272.74	0.46	3.06	Non-critical
	5-8.0			1.89	5.71	
WNW	1-4.0	0.2	272.74	0.46	3.06	Non-critical
W	1-4.0	4.3	272.74	0.46	3.06	3rd highest wave
	5-8.0			1.89	5.71	
	8-12.0			3.95	7.83	
WSW	1-4.0	2.3	245.12	0.45	3.03	Highest wave
	5-8.0			1.85	5.61	
	8-12.0			3.83	7.66	
	12-16.0			6.17	9.37	
SW	1-4.0	22.6	175.70	0.43	2.91	2nd highest wave
	5-8.0			1.70	5.29	
	8-12.0			3.45	7.14	
	12-16.0			5.48	8.67	

NEARSHORE CURRENTS

Nearshore currents generally result from spatial differences in wave energy distributions in the nearshore zone. These differences are associated with the so-called radiation stresses due to waves. Thus, these wave-induced nearshore currents become pronounced where wave energy (which is proportional to the square of wave height) changes drastically such as in the vicinity of the wave breaking zones and zones of wave sheltering such as the shadow zones of breakwaters. They are also induced around areas where wave set-up, or the rise of mean water level due to waves become significant such as crests of submerged structures, and around the wave breaking zone where negative set-up called wave set-down is induced.

For the locations under study, there have been previous reports on the occurrence of nearshore currents, particularly rip currents, which are seaward-directed nearshore currents with high flow intensities, usually occurring near the seabed within a narrow stream width. Rip currents are generally

induced by one or a combination of the following conditions: (1) near-orthogonal approach of incident waves, (2) a pronounced local decrease of depth along the shore, (3) near obstruction along the coastline such as groins, (4) local changes of coastal morphology such as headlands, cuspates, and recessed bays. They are of critical concern to swimmers and the local government as these currents can quickly pull swimmers out to deeper waters outside the safe swimming areas. This section discusses the methodology used to analyze the occurrence of rip currents within and around the areas of concern.

Since wave radiation stress distributions depend on the wave height and wave direction distributions in the nearshore zone, simulations were performed for each offshore prevailing direction under the different wind speeds. In addition to this, constant winds for each direction are applied to the entire domain. Maximum occurring winds and waves were used to simulate the maximum magnitude of currents that may occur. Each direction was assessed individually based on the capacity of the wave to generate rip currents with respect to bathymetric and morphological coastal terrain characteristics.

THRESHOLD CURRENT FOR SAFE SWIMMING AREAS

Safe active swimming areas are to be designated away from areas where strong or significant rip currents are prevalent. The threshold value for such is determined by calculating the largest current magnitude such that a cylindrical body of average human height is stable, both for overtopping and sliding. Drag and inertial forces and moments were calculated in order to derive the threshold value for determination of the safe swimming zones. However, this methodology is deemed to be conservative and is recommended to be further optimized by advanced CFD models on an actual human body to obtain a more accurate estimate. Nonetheless, the definition of “safe” could be subjective to others, thus, concluding in a relative sense would be favorable. Or we may resort to actual physical tests as that of Suga et al (1995) which concluded that a 60-year-old man did not experience any strong feelings of fear when he walked against a water flow as high as his groin with speeds of up to 0.8 m/s. However, intense fear was felt when the flow reached a height of 1 m or a velocity of 1 m/s (Takagi et al, 2016).

MODEL CALIBRATION

The hydrodynamic model was verified using tide data from the nearest tide stations from the study area (NAMRIA, 2016), which are in Balintang and El Nido. Observed data was compared with simulated tidal levels at these stations using conventional statistical methods, plots of which are shown in Figure 6. It is observed that there are no bias for both tide stations and this is supported by a relatively high coefficient of determination (R2), 0.940 and 0.958 for the Balintang and El Nido stations, respectively. Given this, it is reasonable to conclude that the tide levels are well represented by the model.

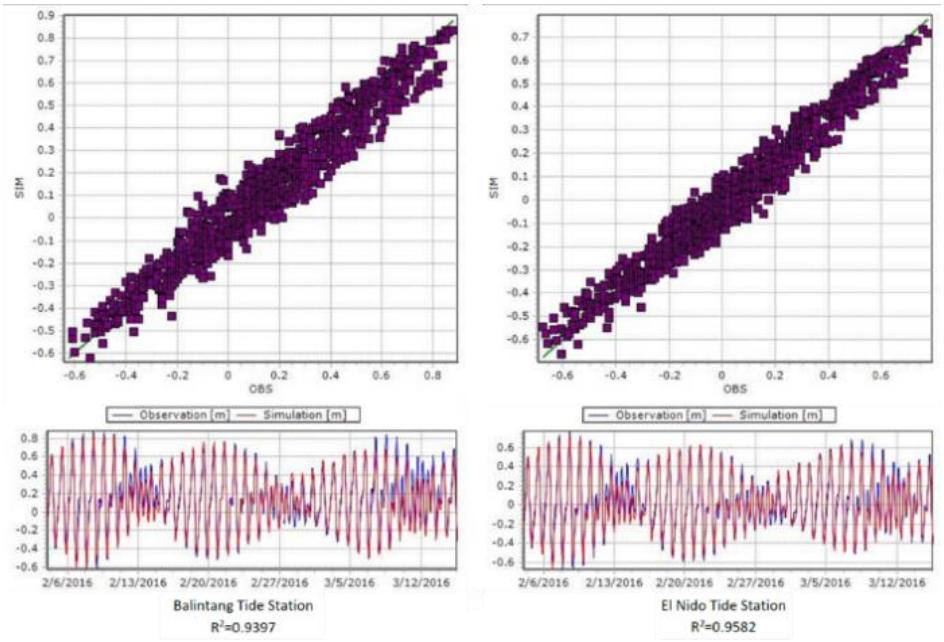

Figure 6. Statistical comparison of simulated tide levels with NAMRIA tide levels at Balintang and El Nido tide stations

RESULTS

Figure 7 and Figure 8 show sample simulation results of rip current formation at peak current intensity for Locations 1 and 2. Table 3 provides a summary of the simulated results for each prevailing direction, indicating occurrences and magnitude of rip currents. Strongest occurrences of rip currents for both locations reach up to 0.35 m/s, which are due to the north incident waves for Location 1. This is considered to be the most open wave approach direction with respect to the coast of Location 1, due to sheltering from the north-westerly directions by several offshore islands i.e. Boayan Island and the shape of the coastline under study. Location 2 on the other hand, is most critical to incident waves coming from the NW direction with respect to rip current generation. This direction is also observed to be perpendicular to the coastline of Location 2.

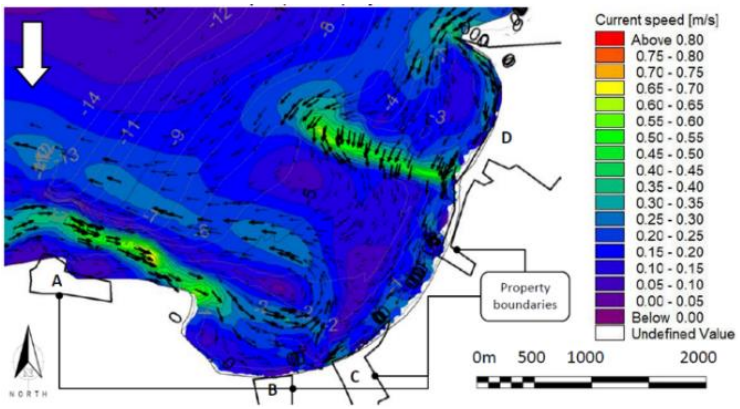

Figure 7. Nearshore currents at peak intensities due to incident waves from the North direction - Location 1

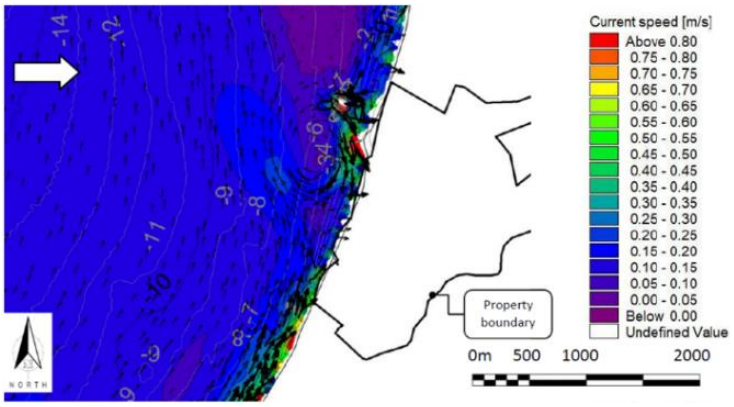

Figure 8. Nearshore currents at peak intensities due to incident waves from the West direction - Location 2

Table 3. Summary of results of nearshore current analysis

Direction	Location 1 (Kemdeng)	Location 2 (Alimanguan)
N	Rip currents (0.3-0.35mps)	Longshore currents to south
NNW	Rip currents (0.15-0.2mps)	
NW	Rip currents (0.15-0.2mps)	Rip currents to the far south of the site (0.35 mps)
WNW	Longshore currents to north	Rip currents at the southern region of the site (0.1mps)
W		Rip currents south of the rocky islet (0.2-0.25mps)
WSW		Longshore currents to north
SW		

From the simulation results, it is observed that the northerly directions contribute more to rip current generation for Location 1, this is due to the geographical location of Boayan Island, covering waves coming from the westerly directions, and the opening from waves coming from the north. However, waves coming from the NNW and NW are reduced in magnitude due to wave refraction. For the case of Location 2, rip currents are more prevalent coming from the north-westerly approach directions. This is also mainly driven by coastline shape and open location of the site. In addition, the coast of Location 2 is closer to the north curvature of the local coastline, while having a rocky islet which impedes the northward momentum of longshore currents generated from onshore wave breaking.

For Location 1, it may be observed that rip currents are generated from incident waves coming from the north to the NW directions. In contrast, for Location 2, rip currents are observed to be generated from incident waves coming from the NW to the west directions. Strongest occurrences of rip currents for both locations reach up to 0.35 m/s. For Location 1, it is mainly due to northerly incident waves penetrating through the opening of the main island and Boayan island. Location 2 on the other hand, is most critical to incident waves coming from the NW direction, mainly due to the orthogonality of wave approach with respect to the coastline.

DETERMINATION OF SAFE AREAS FOR ACTIVE SWIMMING

In order to assess the hazards posed by nearshore generated rip currents, an analysis of the wave and current safety thresholds of humans was undertaken. This analysis was carried out for an average adult, assuming a homogenous and isotropic cylindrical body subjected to rotational and translational forces of drag and inertia on the human body due to the hydraulic loading from waves and currents. It was determined that for an average depth of 1.6 m, a current threshold of 0.16 m/s may be used. This value was determined to be more critical to overturning as compared to sliding by a factor of 8. Based on these results, synthesized threshold current speeds and safe swimming areas were determined. However, it is recommended to conduct further analysis to determine a more efficient threshold value.

Based on the preceding results, current intensities smaller than the threshold current of 0.16 m/s are deemed safe for recreational swimming, while stronger currents greater than this threshold are not safe.

The analysis shows that currents at the determined threshold values is governed by a factor of safety due to overtopping of 1.5, together with a factor of safety due to sliding of 13.2. This means that overtopping is most likely to occur which is considered much more dangerous than sliding out to sea.

For this study, additional safety margin is added to the threshold value of 0.16 m/s, leading to an upper bound of 0.1 m/s for safe areas, and a lower bound of 0.25 m/s for unsafe areas. Also, other areas which are unspecified (h > 2 m) are considered too deep to be safe for recreational swimming. Based on these criteria, the safe swimming areas are shown overlaid on the simulation results in Figure 9, for both Location 1 and Location 2. Additional simulations were undertaken in order to show safe swimming areas for the case of the summer months.

CONCLUSIONS AND RECOMMENDATIONS

Critical longshore and cross-shore current patterns were observed specific to the simulated wave approach directions. Cross-shore currents seen in the simulations indicate the generation of rip currents at specific locations directed out to sea. Generation of these currents are highly depended on three main parameters: (1) the nearshore bathymetry; (2) incident wave approach direction, wherein the frequency is dependent on the season; and (3) the coastline shape, which partially determines the suitable zone where the return flow out to sea occurs. Results also show that generation of rip currents on long continuous coastlines is prevalent, for both sheltered and open beach coasts. However, there is weak correlation of longshore current generation with wave approach almost parallel to the shore.

To assess the hazard posed by nearshore generated rip currents, an analysis of the wave and current safety thresholds of humans was undertaken. This analysis was carried out for an average adult, assuming a homogenous and isotropic cylindrical body subjected to rotational and translational forces of drag and inertia on the human body due to the hydraulic loading from waves and currents. It was determined that for an average depth of 1.6 m, a current threshold of 0.16 m/s may be used. This value was determined to be more critical to overturning as compared to sliding by a factor of 8. Based on these results, synthesized threshold current speeds and safe swimming areas were determined. Although, it is recommended to conduct further analysis to determine a more efficient threshold value.

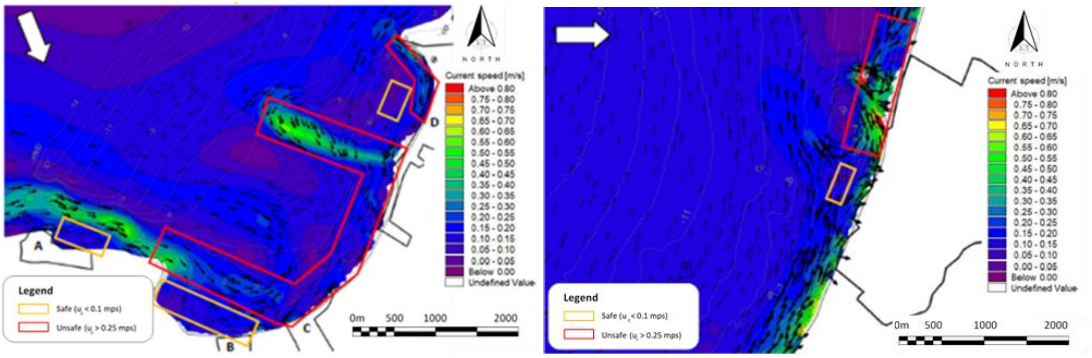

Figure 9. Indicative zones of safe swimming areas along the coastline of Location 1 and 2

ACKNOWLEDGEMENT

The authors would like to acknowledge Engr. Laurenz Luigi B. Cruz for the insightful discussions on hydrodynamic modeling and model calibration which is highly necessary prior to nearshore current analysis.

REFERENCES

Bretschneider, C.L. (1951). Revised wave forecasting curves and procedures. Technical Report No. HE-155047, Inst. of Engineering Research, Univ. of California, Berkeley, 3.

Bretschneider, C.L. (1958). Revision in wave forecasting: deep and shallow water. Proc 9th Conference on Coastal Engineering, 3, 30-67.

Bruneau, Bonneton, Castelle, and Pedreros (2011). Modeling rip current circulations and vorticity in a high-energy mesotidal-macrotidal environment. Journal of Geophysical Res., 116

Coastal Engineering Manual (2006). U.S. Army Corp. of Engineers. http://chl.erdc.usace.army.mil/cem

Cruz, L.L.B., Cruz, E.C., Santos, J.C.E.L. (2018). Coastal engineering design for a stable beach resort development along Davao Gulf. Proceedings, 28th International Ocean and Polar Engineering Conference, 18, 377.

Google TM Earth software. Version 7.1.5.1557. http://earthgoogle.com

MIKE 21 & MIKE 3 Flow Model FM - Hydrodynamic and Transport Module. (2017)

MIKE 21 Spectral Wave Module. (2017)

Philippine Ports Authority (2005). Philippine Ports Standards Manual 2(A).

Takagi, H., Mikami, T., Fujii, D., Esteban, M., Kurobe, S. (2016). Mangrove forest against dyke-break-induced tsunami on rapidly subsiding coasts, Natural Hazards Earth System Sciences, 16, 1629–1638, 2016

Saville, T. Jr. (1954). The effect of fetch width on wave generation. Beach Erosion Board, U.S. Army Corps of Engineers, Tech. Memo No. 45, 1-9.

Suga, K., Uesaka, T., Yoshida, T., Hamaguchi, K., and Chen, Z. (1995). Preliminary study on feasible safe evacuation in flood disaster, Proceedings of hydraulic engineering, The Japan Society of Civil Engineers (JSCE), 39, 879–882, 1995 (in Japanese).

Sverdrup, HU, and Munk, WH (1947). “Wind, sea, and swell: Theory of relations for forecasting,” Hydrographic Office, U.S. Navy Publ. No. 601.